Pis'ma v ZhETF, vol. 93, iss. 11, pp. 752 – 761

ПО ИТОГАМ ПРОЕКТОВ
РОССИЙСКОГО ФОНДА ФУНДАМЕНТАЛЬНЫХ ИССЛЕДОВАНИЙ
Проект РФФИ # 08-02-00243а

Ratchet effects in quantum wells with a lateral superlattice

*E. L. Ivchenko, S. D. Ganichev**

A.F. Ioffe Physical-Technical Institute RAS, 194021 St. Petersburg, Russia

** Terahertz Center, University of Regensburg, 93040 Regensburg, Germany*

Submitted 27 April 2011

Experimental and theoretical work on the ratchet effects in quantum wells with a lateral superlattice excited by alternating electric fields of terahertz frequency range is reviewed. We discuss the Seebeck ratchet effect and a helicity driven photocurrents and show that the photocurrent generation is based on the combined action of a spatially periodic in-plane potential and a spatially modulated light.

1. Introduction. The subject of the present review is terahertz (THz) radiation induced photocurrents in low-dimensional semiconductor systems with spatially periodic noncentrosymmetric lateral potential. Such systems being driven out of thermal equilibrium are able to transport particles even in the absence of an average macroscopic force. This directed transport, generally known as ratchet effect, has a long history and is relevant for different fields of physics, chemistry and biology [1–4].

Ratchet effects whose prerequisites are simultaneous breaking of both thermal equilibrium and spatial inversion symmetry can be realized in a great variety of forms ranging from mechanical systems to molecular motors or electric transport in one-dimensional semiconductor systems. If the directed transport in an asymmetric periodic system is induced by electro-magnetic radiation, it is usually referred to as photogalvanic (or sometimes photovoltaic) effect [5–15], particularly if breaking of spatial inversion symmetry is related to the microscopic structure of the system. Thus, the studies of ratchet effects are naturally related in subject to several hundred experimental and theoretical papers on photogalvanic effects.

While the relationship between ratchet effects driven by alternating electric fields in artificially made macroscopic systems with broken spatial symmetry and light induced photogalvanic effects in noncentrosymmetric crystals and structures is obvious and addressed in several papers [3, 14–17], an impression sometimes arises that these fields are developing independently of each other. Experiments and theory of the ratchet effects induced by THz radiation in low dimensional noncentrosymmetric heterostructures with superimposed macroscopic asymmetric lateral potential described in the present review builds a solid bridge between the two fields and sets up a base for the reciprocation of ideas. In particular, the recently observed Seebeck ratchet caused by electron gas heating under absorption of THz radiation [17], provides an evidence that ratchet effects can be induced even by unpolarized radiation and are similar to the widely discussed thermal noisy transport [1–4, 18–20].

We start the review introducing the basic concepts of ratchet effects. Then in Sec. 3 we give a short overview on the structures used so far for the study of THz radiation induced ratchet effects in semiconductor nanostructures with a lateral one-dimensional potential. In Sec. 4 we perform the symmetry analysis and obtain the polarization dependence of photocurrent. In Sec. 5 we present basics of the kinetic theory of ratchet effect and derive analytical expressions for the Seebeck and polarization-dependent photocurrents. The experimental results are presented and discussed in Sec. 6.

2. Basic concepts. For presenting basic concepts and describing the fundamental phenomena, the transport of a particle in the ratchet is usually modeled by one-dimensional (1D) Newton's equation of motion

$$m\,(\ddot{x} + \eta \dot{x}) = F(x,t) + \zeta(t). \qquad (1)$$

Here, $x \equiv x(t)$ is the particle coordinate, m is its effective mass, dots indicate time derivatives, η is the viscous friction coefficient, $F(x,t)$ is the ratchet force related to the ratchet potential $V(x,t)$ by $F(x,t) = -\partial V(x,t)/\partial x$,

ζ is a randomly fluctuating thermal-noise force. The ratchet force is assumed to be periodic in space with period d and vanish after averaging in space and time. The force ζ is modeled by a Gaussian noise of vanishing mean, $\langle\xi(t)\rangle = 0$, satisfying the fluctuation- dissipation relation $\langle\xi(t')\xi(t)\rangle = 2m\eta k_B T\delta(t'-t)$ with T being the absolute temperature, in the following the Boltzmann constant k_B is set to unity. The state variable x is referred to an effective "Brownian particle" which in many cases is relevant to the position of true particles. However, this variable can also represent a different type of the system degree of freedom, e.g., the total phase $\varphi(t)$ across the ring in an asymmetric SQUID (superconducting quantum interference device) threaded by a magnetic flux [21]. Very often, the dynamics of small systems is approximately described by an overdamped Langevin equation with $m\ddot{x} \to 0$.

In order to present briefly the simplest ratchet models, we start from the ratchet with the time-independent potential $V(x)$. At thermal equilibrium in spatially periodic potential there is no systematic preferential motion of the particle, $\overline{\dot{x}} = 0$, no matter what are the symmetry properties of $V(x)$. For a potential with broken spatial symmetry (non-existence of a point x_0 where $V(x-x_0) = V(x_0-x)$), a directed transport arises in the system driven away from thermal equilibrium. In the so-called *temperature ratchets* the breaking of equilibrium is achieved by subjecting the system temperature to periodic temporal modulations. In another kind of the temperature ratchets, called also the Seebeck ratchets, the system is driven out of equilibrium by introduction of a space-dependent temperature profile $T(x)$ of the same periodicity d as the potential $V(x)$ [3, 18, 19, 22]. In the latter case both the potential $V(x)$ and the temperature profile $T(x)$ can possess centers of inversion but, in an asymmetric system, these centers must not coincide which means that the space average of the product $T(x)dV(x)/dx$ is nonzero. The next type of ratchets, the *tilting ratchet*, is a system with the function $F(x,t)$ of the form $-dV(x)/dx + F(t)$ where the zero-mean force $F(t)$ is a stochastic or periodic function of time, the former system carries the name *fluctuating force ratchet* and the latter is the *rocking ratchet*, see [3, 23, 24]. In the *pulsating ratchets* the periodic or stochastic non-equilibrium perturbation $F(x,t)$ induces a time-dependent variation of the potential keeping its spatial periodicity. Particularly, in the pulsating *on-off ratchets*, $F(x,t)$ is set to $f(t)dV(x)/dx$ with $f(t)$ taking on only two possible values, one of them being 0 (potential "off"). Another example of time- dependent variation of the potential shape, without affecting its spatial periodicity, is given by

$$F(x,t) = -\frac{dV(x)}{dx} + F(t)P(x), \qquad (2)$$

where $F(t)$ is periodic in time and the periodical functions $V(x)$ and $P(x)$ have the same period d.

As a possible realization of the temperature (Seebeck) ratchet, Blanter and Büttiker [19] proposed to use a superlattice (SL) irradiated by light through a mask of the same period but phase shifted with respect to the SL yielding a directed current due to local electron gas heating. The force $F(x,t)$ acting on free electrons has the form of Eq. (2) where $F(t)P(x) = eE(x,t)$, e is the electron charge, $E(x,t)$ is the electric field of the electromagnetic field, $F(t)$ oscillates in time at the light frequency ω and $P(x) = P(x+d)$ is the in-plane modulation of the electric-field amplitude caused by the mask. The radiation-induced heating of the electrons leads to a periodic temperature profile $T(x)$ and allows the ratchet effect. Thus, the pulsating model (2) can be mapped onto the Seebeck ratchets.

In the recent publications [17, 25, 26] we have reported an experimental realization of the original idea of Blanter and Büttiker, with some modifications. The photocurrent induced by THz radiation has been observed in semiconductor quantum-well structure with a 1D lateral periodic potential induced by etching a noncentrosymmetric grating into the sample cap layer. Hence, the in-plane modulation of the pump radiation appears not via a mask with periodic structures but due to near-field effects of the THz radiation propagating through the grating. In this system the electron moves freely in two dimensions, x and y, where we use the Cartesian coordinate frame (x,y,z) with the z-axis parallel to the structure growth direction. This means that, in terms of the classical stochastic dynamics, the scalar equation (1) should be replaced by the similar vector equation for the two-dimensional (2D) position vector $\mathbf{r}$ with the components x, y and the two-component force

$$\mathbf{F}(x,t) = -\frac{dV(x)}{dx}\ \mathbf{o}_x + e\mathbf{E}(x,t), \qquad (3)$$

where $V(x)$ is the ratchet potential, $\mathbf{o}_x$ is the unit vector along the x axis, and $\mathbf{E}(x,t)$ is the in-plane time- and x-dependent electric field with two components $E_x(x,t)$ and $E_y(x,t)$. Since the light-induced Seebeck ratchet current arises due to the heating this current is light-polarization independent. It can be shown, however, that in addition to the Seebeck ratchet effect, the force (3) induces a polarization- dependent directed transport sensitive to the radiation circular polarization (*circular ratchet*) and linear polarization in the axes x', y' rotated by $45°$ with respect to the axes x, y (*linear ratchet*)

[17, 26]. The mechanisms of these ratchet effects are unrelated to the electron-gas heating.

3. Experimentally studied lateral structures. Ratchet effect crucially depends on the structure's design. Thus, to be specific in the discussion of phenomenological (Sec. 4) and microscopic (Sec. 5) theory, we first briefly introduce the structures under study. Experimentally THz radiation induced ratchet effects in lateral low-dimensional semiconductor structures have been observed employing two types of lateral SL gratings [17, 25, 26]. The gratings have been prepared on molecular-beam epitaxy (001)-grown Si-δ-doped n-type $GaAs/Al_xGa_{1-x}As$ heterostructures with electron mobilities and carrier densities at room temperature in the range of $3{-}6\cdot10^3\,\mathrm{cm}^2/\mathrm{Vs}$ and $10^{11}{-}10^{12}\,\mathrm{cm}^{-2}$, respectively. At room temperature the electron mean free path l_e is about $0.5\,\mu$m and, hence, the condition $l_e \ll d$ holds. The studied superlattices mainly differ in the design of the gratings providing the asymmetric potential.

The first type of superlattice (ST1) consists of asymmetrically etched grooves oriented along the [100] cubic direction with a SL period d of 2.5 μm. Grooves with 0.5 μm width were obtained by electron beam lithography and subsequent reactive ion etching using $SiCl_4$. Care was taken not to etch through the 2D-electron system. A corresponding sketch of the grating and an electronic micrograph are shown in Figs. 1b and d, respectively. The asymmetric modulation of the lateral potential comes from the shape of the grooves: the average depth on the right side of a groove is smaller than that on the left side. The degree of asymmetry in these structures is due to anisotropic etching and may vary from sample to sample being dependent on the orientation of the grooves with respect to crystallographic axes. For the photoelectric experiments we used $5\times5\,\mathrm{mm}^2$ square shaped samples oriented along the [110]- and [1$\bar{1}$0]-directions. To measure photocurrents, pairs of ohmic contacts were alloyed in the middle of each sample edge.

The second set of superlattices (ST2) allows much better control of the asymmetry and enables both transport and photocurrent measurements in one and the same device. The latter is achieved by using of a Hall bar geometry. Here the SL is produced by e-beam lithography and deposition of micropatterned gate fingers using 15 nm Ti and 120 nm Au. The schematics of the gate fingers, consisting of stripes having three different widths A = 1 μm, B = 0.6 μm and C = 0.3 μm with ratio A:B:C = 10:6:3, and separated by A, B, and C, is shown in Fig. 1c and a corresponding electron micrograph in Fig. 1e. This asymmetric supercell is repeated to generate an asymmetric but periodic potential super-

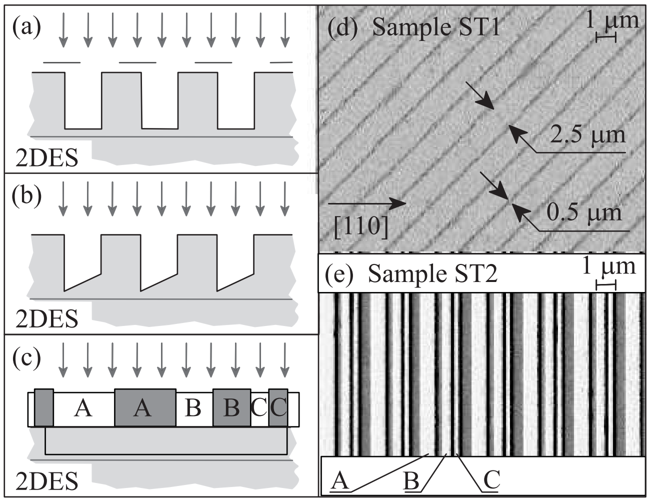

Fig. 1. Sample design. (a) Blanter and Büttiker's geometry. (b) The experimental geometry of the first set of samples (type 1, ST1) with an asymmetric groove profile. (c) The geometry of the second set of samples (type 2, ST2) with supercells ABCABC... of metallic stripes on top of the sample. (d) Electron micrograph of the first set of samples (ST1). (e) Electron micrograph of the second set of samples (ST2). Here, the widths of the patterns A, B and C are 1 μm, 0.6 μm and 0.3 μm, respectively

imposed upon the 2D electron system. The asymmetric supercells $ABCABC$... are patterned on a $500\cdot140\,\mu\mathrm{m}^2$ area and generate a strain-induced potential in the 2DES with a period d of $3.8\,\mu$m. The gate fingers, all connected and grounded, are oriented along the y-direction, perpendicularly to the Hall bar.

In order to compare the data of modulated and unmodulated 2D electron systems reference samples have been used for both types of SL. As reference samples for ST1 unpatterned samples R1 and/or structures R2 with grooves very close to $\langle 110\rangle$ have been used. The cross section of the latter grooves is rather symmetric. The reference sample for ST2 set of structures have been obtained by preparation of Hall bars consisting of a patterned region as well as of an unpatterned reference part.

4. Symmetry analysis. In this section, we will analyze symmetry restrictions imposed on the polarization dependence of the ratchet currents. The SL shown in Fig. 1 have the point group symmetry C_s consisting of the identity element and the reflection σ in the plane perpendicular to the channels (y-axis). It follows then that the current density components j_x, j_y are related to components of the polarization unit vector $\mathbf{e} = \mathbf{E}_0/|\mathbf{E}_0|$ by four linearly independent coefficients

$$
\begin{aligned}
j_x &= \bar{I}[\chi_1 + \chi_2(|e_x|^2 - |e_y|^2)], \qquad (4)\\
j_y &= \bar{I}[\chi_3(e_x e_y^* + e_y e_x^*) - \gamma P_{\mathrm{circ}}\hat{e}_z]\,,
\end{aligned}
$$

where $P_{\rm circ}\hat{\mathbf{e}} = {\rm i}(\mathbf{e}\times\mathbf{e}^*)$, $\bar{I}$ is the average light intensity Note that in the described geometry the light propagation direction and the z axis are anti-parallel causing the minus sign in the second equation of Eqs. (4). The Seebeck ratchet effect is connected to the coefficient χ_1, while the remaining three coefficients describe the linear (χ_2, χ_3) and circular (γ) ratchet effects.

Equations (4) should be compared to the ones of corresponding unpatterned samples, called reference samples below, or structures with a symmetric potential. One-sided modulation-doped QWs, grown along the crystallographic [001] direction of zinc-blende-lattice semiconductors have point-group symmetry C_{2v} which excludes in-plane currents for normal incidence where $E_{0z} = 0$, in contrast to the ratchet currents (4), allowed for this geometry. Under oblique incidence, the reference samples admit directional photogalvanic electric currents perpendicular to the plane of incidence [8]

$$
\begin{aligned}
j_{x'} &= I[\chi_{x'x'z}\,(e_{x'}e_z^* + e_z e_{x'}^*) + \gamma_{x'y'}P_{\rm circ}\hat{e}_{y'}]\,, \qquad (5)\\
j_{y'} &= I[\chi_{y'y'z}\,(e_{y'}e_z^* + e_z e_{y'}^*) + \gamma_{y'x'}P_{\rm circ}\hat{e}_{x'}]\,,
\end{aligned}
$$

which are caused by the lack of an inversion center in the reference samples at the atomic level. Here, x' and y' denote the axes $[\bar{1}10]$ and [110], respectively, $\boldsymbol{\chi}$ and $\boldsymbol{\gamma}$ are a third-order tensor and a second-order pseudotensor describing the linear (LPGE) and circular (CPGE) photogalvanic effects, respectively. Equations (5) show that in reference samples a photocurrent can be generated only at oblique incidence (z-component of the radiation electric field is needed). This is in contrast to the asymmetric lateral structures where the current given by Eqs. (4) reaches a maximum at normal incidence.

Since the lateral superstructure is responsible for the photocurrents observed at normal incidence, see Sec. 4, then one can, while developing a theory of the normal-incident currents, ignore the initial (microscopic) symmetry C_{2v} of the reference heterostructure, disregard mechanisms of photocurrents related to the lack of an inversion center in the unstructured sample and rely only on the symmetry of the superstructure potential $V(x)$ and the in-plane intensity modulation. In this case Eqs. (4) can be applied for any orientation of the axes x, y irrespectively to the crystallographic directions $[1\bar{1}0]$, [110]. At oblique incidence, the photocurrent can be naturally described by a sum of superstructure-induced and intrinsic contributions, Eqs. (4) and (5).

In the both patterned samples ST1 and ST2, obliquely incident light generates both the ratchet current (4) and the photogalvanic current (5). This allows to compare the contributions to the photocurrents due to the lack of inversion symmetry on the atomic (intrinsic mechanisms) and on the micron scale (periodic grating) experimentally.

5. Kinetic theory. We consider a quantum well (QW) structure modulated by a 1D periodic lateral potential $V(x)$. In addition to the static potential $V(x)$, the 2D electron gas is subjected to the action of an in-plane time-dependent electric field $\mathbf{E}(x,t) = \mathbf{E}_\omega(x)e^{-{\rm i}\omega t} + {\rm c.c.}$ with the amplitude $\mathbf{E}_\omega(x)$ modulated along the x axis with the same period as the static lateral potential. In general, the modulated field amplitude and lateral potential can be presented in the form

$$
\begin{aligned}
\mathbf{E}_\omega(x) &= \mathbf{E}_0\left[1 + \sum_{n=1}^{\infty} h_n \cos\left(nqx + \varphi_{E,n}\right)\right], \qquad (6)\\
V(x) &= \sum_{n=1}^{\infty} V_n \cos\left(nqx + \varphi_{V,n}\right),
\end{aligned}
$$

where $q = 2\pi/d$. Hereafter, for simplicity, we take the modulation in the form

$$
\begin{aligned}
\mathbf{E}_\omega(x) &= \mathbf{E}_0[1 + h_1 \cos\left(qx + \varphi_E\right)]\,, \qquad (7)\\
V(x) &= V_1 \cos\left(qx + \varphi_V\right).
\end{aligned}
$$

Presenting the final results we will show what form they take for the general modulation (6).

We will describe the ratchet effects by using the classical Boltzmann equation for the electron distribution function $f_{\mathbf{k}}(x,t)$, namely,

$$
\left(\frac{\partial}{\partial t} + \mathbf{v}_{\mathbf{k},x}\frac{\partial}{\partial x} + \frac{\mathbf{F}(x,t)}{\hbar}\frac{\partial}{\partial \mathbf{k}}\right) f_{\mathbf{k}}(x,t) + Q_{\mathbf{k}} = 0. \qquad (8)
$$

Here, $\mathbf{k} = (k_x, k_y)$ and $\mathbf{v}_{\mathbf{k}} = \hbar\mathbf{k}/m$ are the 2D electron wave vector and velocity, the force $\mathbf{F}(x,t)$ is given by Eq. (3), and $Q_{\mathbf{k}}$ is the collision integral responsible for electron momentum and energy relaxation. Equation (8) is valid for a weak and smooth potential satisfying the conditions $|V(x)| \ll \varepsilon_e$ and $q = 2\pi/d \ll k_e$, where k_e and ε_e are the typical electron wave vector and energy, the latter being much larger than the photon energy $\hbar\omega$. The quantity of central interest is the average electron current

$$
\mathbf{j} = 2e\sum_{\mathbf{k}} \mathbf{v}_{\mathbf{k}} \bar{f}_{\mathbf{k}}, \qquad (9)
$$

where the factor 2 takes into account the electron spin degeneracy and the bar means averaging over the spatial coordinate x and time t. The ratchet currents can be obtained by solving the kinetic equation (8) in third order perturbation theory, i.e., second order in the electric-field amplitude and first order in the static lateral potential. In this work, we use the collision integral $Q_{\mathbf{k}}$

in the convenient form of a sum of the elastic scattering term $Q_{\mathbf{k}}^{(\mathrm{el.sc})}$ and the energy relaxation term Q_ε. The former is taken in the simplest form

$$Q_{\mathbf{k}}^{(\mathrm{el.sc})} = \frac{f_{\mathbf{k}}(x,t) - \langle f_{\mathbf{k}}(x,t)\rangle}{\tau}, \tag{10}$$

where the brackets mean the average over the directions of $\mathbf{k}$, and τ is the momentum scattering time assumed to be constant. The term Q_ε is treated in the approximation of effective temperature.

The electron distribution function is expanded in powers of the light electric-field up to the second order,

$$f_{\mathbf{k}}(x) = f_{\mathbf{k}}^{(0)}(x) + f_{\mathbf{k}}^{(1)}(x,t) + f_{\mathbf{k}}^{(2)}(x,t), \tag{11}$$

where $f_{\mathbf{k}}^{(0)}(x)$ is the equilibrium distribution function. Here we consider the limit of high temperatures and assume that the electron gas obeys a non-degenerate statistics. Then, retaining terms of zero and first orders in the lateral potential, we can approximate the equilibrium distribution function by

$$f_{\mathbf{k}}^{(0)}(x) = \left(1 - \frac{V(x)}{T_0}\right)\exp\left(\frac{\mu_0 - \varepsilon_{\mathbf{k}}}{T_0}\right), \tag{12}$$

where $\varepsilon_{\mathbf{k}} = \hbar^2 k^2/2m$, T_0 is the equilibrium temperature and μ_0 is the chemical potential.

The first-order correction is time-dependent and can be written as a sum of two complex-conjugate monoharmonic terms $f_{\mathbf{k}}^{(1)}(x,t) = e^{-\mathrm{i}\omega t} f_{\mathbf{k}\omega}^{(1)}(x) + \text{c.c.}$ For the second order correction, it is sufficient to retain the time-independent contribution $f_{\mathbf{k}}^{(2)}(x) \equiv \xi_{\mathbf{k}}(x)$ only and to reduce Eq. (9) to

$$\mathbf{j} = 2e \sum_{\mathbf{k}} \mathbf{v}_{\mathbf{k}}\ \bar{\xi}_{\mathbf{k}}\,. \tag{13}$$

By the successive iteration of the kinetic equation, substitution of $f_{\mathbf{k}}(x)$ into Eq. (9) and summing over $\mathbf{k}$ we arrive at

$$\mathbf{j} = \mu_e \left\{ \overline{\delta N(x)\frac{dV(x)}{dx}}\mathbf{o}_x + 2|e|\mathrm{Re}\overline{[\mathbf{E}_\omega^*(x)\delta N_\omega(x)]} \right\}. \tag{14}$$

Here μ_e is the electron mobility $|e|\tau/m^*$ and we introduced the spatially- modulated electron densities

$$\delta N(x) = 2\sum_{\mathbf{k}} \xi_{\mathbf{k}}(x)\,, \quad \delta N_\omega(x) = 2\sum_{\mathbf{k}} f_{\mathbf{k}\omega}^{(1)}(x). \tag{15}$$

The further development of the theory is based on additional assumptions: (i) the energy relaxation time τ_ε is assumed to exceed the time τ and the inverse frequency ω^{-1}, (ii) the electron mean free path $l_e = v_T\tau$ and energy diffusion length $l_\varepsilon = v_T\sqrt{\tau\tau_\varepsilon}$ are both small compared with the SL period d, where v_T is the thermal velocity $\sqrt{2T/m}$, (iii) we neglect the influence of ac diffusion on the first-order amplitudes $f_{\mathbf{k}\omega}^{(1)}(x)$ which is valid if $v_T q \ll \omega$. On the other hand, no restrictions are imposed on the value of the product $\omega\tau$.

The first term in the right-hand side of Eq. (14) describes the Seebeck ratchet photocurrent. To calculate this current we need to find a static correction $\delta N(x)$ of the spatially modulated electron density. This correction, together with local non-equilibrium temperature $T(x)$, current density j_x and energy flux density $\mathcal{J}(x)$, satisfy the following macroscopic equations

$$j_x = \mu_e\left\{N(x)\frac{dV(x)}{dx} + \frac{d}{dx}[T(x)N(x)]\right\}, \tag{16}$$

$$\mathcal{J} = [2T(x) + V(x)]\,\frac{j_x}{e} + \frac{\mu_e}{e}N(x)\frac{dT^2(x)}{dx}\,,$$

$$\frac{d\mathcal{J}}{dx} = \hbar\omega G(x)N(x) - \frac{T(x)-T_0}{\tau_\varepsilon}N(x)\,,$$

and $dj_x/dx = 0$. Here, we introduced the energy relaxation time τ_ε and the generation rate $G(x)$ defined as the Drude absorption rate per particle,

$$G(x) = \frac{4\pi e^2}{mn_\omega}\ \frac{\tau}{1+\omega^2\tau^2}\ \frac{I(x)}{\hbar\omega},$$

where the light intensity is defined by

$$I(x) = \frac{cn_\omega}{2\pi}(|E_{\omega,x}(x)|^2 + |E_{\omega,y}(x)|^2)\,,$$

c is light velocity in vacuum, n_ω is the refractive index.

Under homogeneous optical excitation, $G(x) \equiv G_0$, Eqs. (16) have the following solution

$$T = T_0 + \hbar\omega G_0\tau_\varepsilon\,,\ N(x) = N_0 e^{-V(x)/T}\,,$$

where N_0 is x-independent. For this solution, both j_x and $\mathcal{J}$ vanish. The current j_x becomes nonzero only if the generation rate G varies spatially. For the simple spatial modulation (7) of the electric field with a small coefficient h_1, we have $G(x) = G_0[1+2h_1\cos(qx+\varphi_E)]$. Neglecting the energy diffusion term in Eqs. (16) we obtain that the steady-state generation produces a stationary periodic electron temperature $T(x)$ with $T(x) - T \equiv \equiv \delta T(x) = \tau_\varepsilon\hbar\omega[G(x) - G_0]$. From the first equation (16) it follows that this temperature modulation is accompanied by a light-induced periodic correction to the electron density $\delta N(x) \approx -N_0\delta T(x)/T$.

For the lateral potential given by Eq. (7) where the symmetry of the system is broken by a phase shift between $V(x)$ and $\Theta(x)$, the final result reads

$$j_x = \chi_1^{\mathrm{S}}\bar{I} = \zeta\frac{4\pi e^2}{\hbar c n_\omega}\frac{\hbar q}{m^*}\frac{\mu_e N_0\tau\tau_\varepsilon}{1+\omega^2\tau^2}\frac{\bar{I}V_1}{T}, \tag{17}$$

where $\zeta = h_1 \sin(\varphi_V - \varphi_E)$ is the asymmetry parameter related to the inhomogeneous photoexcitation. For a more complicated spatial modulation (6), the product $\zeta q V_1$ should be replaced by $\sum_n nqV_n h_n \sin(\varphi_{V,n} - \varphi_{E,n})$. The Seebeck ratchet current (17) is polarization independent and increases with decreasing temperature.

Now we turn to the polarization dependent mechanisms of the currents and discuss the linear and circular ratchet effects described in Eqs. (4) by the terms proportional to χ_2, χ_3 and γ. We show that these ratchet currents can also be generated in a lateral SL with the out-of-phase periodic potential $V(x)$ and electric field $\mathbf{E}_\omega(x)$. For this purpose we consider the second term in Eq. (14). The oscillation $\delta N_\omega(x)$ entering (14) and defined by Eq. (15) satisfies the continuity equation

$$-i\omega \delta N_\omega(x) + \frac{\partial j_{\omega,x}(x)}{\partial x} = 0\,, \tag{18}$$

where $j_{\omega,x}(x)$ is the amplitude of current oscillations at frequency ω. Since $\overline{\delta N_\omega(x)} = 0$ then, in order to calculate the current given by the second term in Eq. (14), it is sufficient to find a contribution to $\delta N_\omega(x)$, linear in the lateral potential and a *non-modulated* electric field E_{0x}.

The function $f^{(1)}_{\mathbf{k}\omega}(x)$ is conveniently rewritten as

$$f^{(1)}_{\mathbf{k}\omega}(x) = \frac{e\mathbf{E}_0\mathbf{v}_\mathbf{k}\tau_\omega}{k_B T} f^{(0)}_\mathbf{k}(x) + F_{\mathbf{k}\omega}(x), \tag{19}$$

where $\tau_\omega = \tau/(1 - i\omega\tau)$. Neglecting the ac diffusion and calculating the correction $F_{\mathbf{k}\omega}(x)$ in first order in the lateral potential we find after summation over $\mathbf{k}$

$$\delta N_\omega(x) = \frac{ie\tau_\omega N_0}{\omega m^* k_B T} \frac{dV(x)}{dx} E_{0x}. \tag{20}$$

Substituting Eq. (20) to Eq. (14) and averaging over x we obtain the ratchet photocurrents, which, together with the polarization independent current (17), can be written as

$$j_x = \bar{I}[\chi_1 + \chi_2(|e_x|^2 - |e_y|^2)], \tag{21}$$
$$j_y = \bar{I}[\chi_3(e_x e_y^* + e_y e_x^*) - \gamma P_{\mathrm{circ}} \hat{e}_z],$$

with coefficients

$$\chi_2 = \chi_3 = -\omega\tau\gamma, \quad \chi_1 = \chi_1^{\mathrm{S}} - \omega\tau\gamma \tag{22}$$

and

$$\gamma = \zeta \frac{\pi e^2}{\hbar c n_\omega} \frac{\hbar q}{m^*} \frac{V_1}{k_{\mathrm{B}} T} \frac{\mu_e N_0 \tau}{\omega(1 + \omega^2\tau^2)}\,, \tag{23}$$

being in full agreement with the phenomenological Eqs. (4).

Figure 2 illustrates the generation of circular-ratchet photocurrent under circularly polarized excitation. We choose the phases $\varphi_V = 0$, $\varphi_E = -\pi/2$ in which case one has $V(x) = V_1 \cos qx$ and

$$E_x(x,t) = 2\cos\omega t\; E_{0x}(1 + h_1 \sin qx),$$
$$E_y(x,t) = 2\sin\omega t\; E_{0y}(1 + h_1 \sin qx)$$

with $E_{0y} = E_{0x}$. The equilibrium electron concentration can be represented by $N_0(x) = N_0 + \delta N_0(x)$ with $\delta N_0(x) = -(V_1 N_0/T_0)\cos qx$. If the diffusion is neglected then the spatially modulated part of the current induced by the field E_x reads

$$\delta j_x(x,t) = \frac{\mu_e N_0}{1 + \omega^2\tau^2} \frac{V(x)}{T_0} \cdot 2(\cos\omega t + \omega\tau \sin\omega t) E_{0x}.$$

By using the continuity equation (18) we find the pulsating profile of electron concentration

$$\delta N(x,t) = \frac{\mu_e N_0}{1 + \omega^2\tau^2} \frac{qV_1}{\omega T_0} \cdot 2(\sin\omega t - \omega\tau \cos\omega t) E_{0x}.$$

For the circularly polarized radiation, it suffices to take into account only the first term in the brackets because the second term contributes not to γ but to χ_3. Lengths of horizontal arrows in Fig. 2a indicate values of $\delta j_x(x,t)$ at the moment $t = 0$. One can see that the carriers are pushed to the point $x = d/4$ and off the point $x = 3d/4$. At the moment $t_0 = \pi/(2\omega)$ (one fourth of the period) both the concentration contrast and the electric field E_y become the largest. Since the profiles of modulation of $\delta N(x, t_0)$ and $E_y(x, t_0)$ coincide, the electric current $j_y(t) = |e|\mu_e \overline{\delta N(x,t) E_y(x,t)}$ in the y direction reaches its maximum value, see vertical arrows in Fig. 2b. At the moment $2t_0$ the electric field E_x changes its sign and so does the current δj_x. But since $E_y(3t_0) = -E_y(t_0)$, the current $j_y(3t_0)$ coincides with $j_y(t_0)$ and the average j_y value is nonzero and described by γ.

6. Experimental results and discussion. The experiments on ratchet effects in lateral superlattices have been performed applying alternating THz fields of far-infrared laser radiation [17, 25, 26]. A high power pulsed molecular THz laser [27, 28] has been used as a radiation source in the spectral range between 90 μm and 280 μm. The power of $P \simeq 5$ kW was controlled by the linear photon drag detector [29]. The corresponding photon energies $\hbar\omega$ lie in the range of 13.7 meV to 4.4 meV. For this radiation, the photon energies are less than the energy gap or energy separation between size quantized subbands in 2DEG so that in experiments carried out at room temperature the radiation excites only indirect optical transitions (Drude absorption) in the lowest subband. Radiation could be applied at both

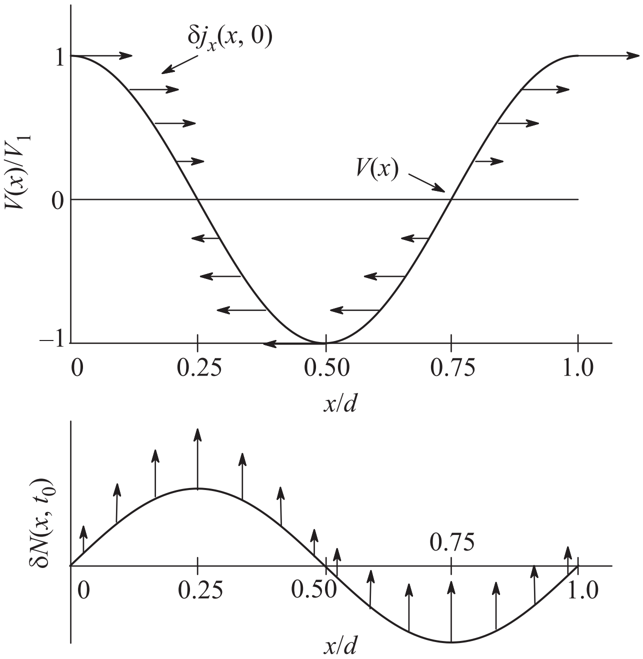

Fig. 2. Schematic illustration of the circular ratchet effect caused by circularly polarized light at normal incidence. (a) Solid curve shows the ratchet potential $V(x)$. Horizontal arrows indicate the direction and value of the oscillating space-modulated current $j_x(x,t)$ induced by the electric field E_x at the moment $t = 0$. (b) Solid curve: The space-modulated part $\delta N(x,t)$ of the electron density at the one-fourth of period, $t = t_0 = \pi/(2\omega)$. The profile of the field y-component E_y at this moment coincides with that of δN. Vertical arrows: The electric current induced by E_y at $t = t_0$ and related to the modulation $\delta N(x,t_0)$

normal incidence ($\theta_0 = 0$) and oblique incidence with the angle of incidence θ_0 varying from $-30°$ to $30°$. The current generated by THz light in the unbiased samples was measured via the voltage drop across a 50 Ω load resistor in a closed-circuit configuration. The voltage was recorded with a storage oscilloscope.

As it follows from the discussion above the Seebeck ratchet can be induced even by unpolarized light. By contrast, the linear and circular ratchet effects require polarized radiation. Optically pumped molecular lasers emit linearly polarized radiation whose orientation is determined by the polarization of the pump radiation and in the reviewed experiments was set to $\mathbf{E} \parallel \mathbf{y}$ [9]. To study polarization behaviour of the radiation induced currents the polarization of the laser beam has been modified applying crystal quartz $\lambda/4$- and $\lambda/2$-plates.

By rotating the $\lambda/4$ plate, one transfers the linear into elliptical polarization. The polarization states are directly related to the angle φ between the initial linear polarization of the laser light and the optical axis of the plate, resulting in $P_{\rm circ} = \sin 2\varphi$ for the degree of circular polarization and for the bilinear combinations of the polarization vector components

$$S_1(\varphi) \equiv |e_x|^2 - |e_y|^2 = -\cos^2 2\varphi, \qquad (24)$$
$$S_2(\varphi) \equiv e_x e_y^* + e_y e_x^* = -\frac{1}{2}\sin 4\varphi.$$

If the plane of polarization of linearly polarized light incident upon a $\lambda/2$ plate is at an angle $\varphi_{\lambda/2}$ with respect to the slow axis the plane of polarization of the transmitted light is rotated by an angle $\alpha = 2\varphi_{\lambda/2}$ and the above bilinear combinations are given by

$$S_1(\alpha) = -\cos 2\alpha, \quad S_2(\alpha) = -\sin 2\alpha. \qquad (25)$$

We note, that parameters S_1, S_2 and $S_3 \equiv P_{\rm circ}$ represent the radiation Stokes parameters and describe the degree of linear polarization in the coordinate axes x, y (S_2), within the system rotated about an angle of 45° (S_1) and radiation helicity ($P_{\rm circ}$), respectively [30].

Experimental study of the THz radiation induced ratchet effects in lateral superlattices requires a careful choice of the experimental geometry. The challenge is to exclude contributions of the photogalvanic effects [31], which are caused by the microscopic asymmetry of the elementary excitation/scattering processes and can be excited even in unpatterned samples. Fortunately, for structures prepared on the (001)-oriented substrate the reduction of symmetry resulting from the asymmetric lateral potential provides a straightforward way to achieve this goal. Indeed, while the photogalvanic effects in such a structures are forbidden at normal incidence the ratchet effects due to SL in the same geometry achieve their maximum.

Following [17, 25, 26] we focus on experiments aimed to the THz radiation induced ratchet effects. We start with Hall bar samples, ST2, in which the asymmetric lateral potential has been obtained by means of micropatterned gate fingers. The structure consists of the patterned and unpatterned areas (see inset in Fig. 3). In unpattenned area a photocurrent is only observed at oblique incidence. This finding is in agreement with the discussion above underlining that ratchet effects do not occur in unpatterned structures. In the patterned part of the sample, however, a remarkable photocurrent J_x has been observed at normal incidence [26]. As shown in Fig. 3, the current, which flows perpendicularly to the asymmetric stripes, strongly depends on the azimuth angle α of the light's polarization defined above and can be well fitted by

$$J_x = J_1 + J_2 S_1(\alpha). \qquad (26)$$

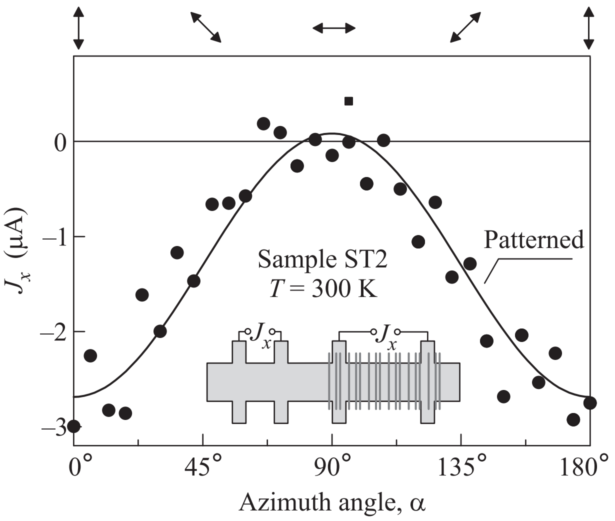

Fig. 3. Photocurrent J_x measured at sample ST2 with asymmetric stripes ABC... as a function of the azimuth angle α. The data are obtained at normal incidence by radiation with wavelength of $\lambda = 280$ μm and power $P \approx 9$ kW. The current induced in the structured part by linearly polarized radiation is well fitted by Eq. (26), see also Eq. (21). The inset displays the design of the Hall bar with the structured and the unpatterned part. Arrows on top indicate the polarization corresponding to various values of α

This is fully in line with the theory of the ratchet effect discussed above and given by Eqs. (4) and (21). Our observation demonstrates that an asymmetric periodic potential can be controllably introduced by the ABC gate. We note that in this sample the interplay of the polarization independent Seebeck photocurrent J_1 (Eq. (17)) and linear ratchet photocurrent proportional to J_2 [or to the coefficient χ_2 in Eqs. (21)] yields a maximum of the signal for the radiation electric field aligned perpendicular to the direction of modulation.

The Hall bar design of ST2 structures makes possible an independent control of the modulation of 2DES potential. Figure 4 shows the magnetic field dependence of the longitudinal resistance ρ_{xx} measured in the patterned and unpatterned (see the inset) areas. The data are obtained at low temperatures and display the pronounced Shubnikov-de Haas oscillations for unpatterned part of the sample. In the patterned part of the sample, by contrast, the Weiss-oscillations [32] are detected. This observation is a clear signature of the presence of a weak periodic potential. In ST2 structures the mean free path l_e in the superlattice device at low temperature is about 9 μm and hence longer than the period of the SL as well as much longer than the average distance between neighboring finger strips. In this limit the periodic potential causes $1/B$ periodic resistance oscillation where minima are given by the condition

$$2R_{\mathrm{C}} = \left(\lambda_{\mathrm{C}} - \frac{1}{4}\right) d\,,\ \lambda_{\mathrm{C}} = 1, 2, 3... \qquad (27)$$

Here, $2R_{\mathrm{C}}$ is the semi-classical cyclotron orbit diameter and λ_{C} is the oscillation index. Such commensurability (or Weiss-oscillations) are clearly visible at low magnetic fields of the trace measured in the superlattice part of the sample, as presented in Fig. 4. The SL period d

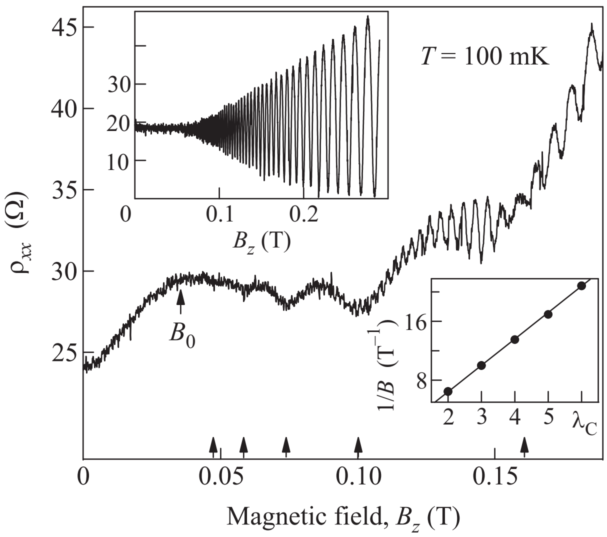

Fig. 4. Longitudinal resistance ρ_{xx} in the modulated part of the Hall bar sample ST2. At low B, $1/B$ periodic commensurability oscillation indicate the presence of a weak periodic potential. The $1/B$ periodicity of the low-field oscillations is evident from the inset where the oscillation index λ_{C} is plotted vs. the resistance minima position $1/B$ in the bottom right inset. The upper left inset shows the Shubnikov-de Haas oscillations measured at 100 mK in the unpatterned reference section of the ST2 sample

extracted from the Weiss-oscillations is about 570 nm and agrees with one of the Fourier components of the asymmetric periodic potential.

The polarization independent Seebeck photocurrent J_1 (Eq. (17)) and linear ratchet photocurrent proportional to J_2 [or to the coefficient χ_2 in Eqs. (21)] have also been observed in the other set of the lateral structures, ST1, with the asymmetric potential caused by the asymmetric periodic grooves. Figure 5 shows the photocurrent generated at normal incidence in sample ST1 as a function of the the azimuth angle α (see panel a) and angle φ indicating the helicity (see panel b). The current is measured at an angle of 45° with respect to the axes

x and y and can be well fitted by an equal superposition of j_x and j_y of Eqs. (21) yielding

$$J = J_1 + J_2 S_2(\alpha) + J_3 S_1(\alpha) \quad (28)$$

and

$$J = J_1 + J_2 S_2(\varphi) + J_3 S_1(\varphi) + J_{\mathrm{C}} P_{\mathrm{circ}}(\varphi). \quad (29)$$

Here, the fitting parameters J_j $(j = 1, 2, 3)$ and J_{C} are related to the coefficients χ_j and $-\gamma$ in Eq. (21) by the factor $\bar{I}/\sqrt{2}$. We emphasize that, as expected from the theory, fitting parameters J_j used for the data shown in the panel *a* are the same as the ones used in the panel *b*. Also here, no photocurrent is observed in reference samples excited at normal incidence.

Figures 3 and 5 demonstrate that the dominant contribution to the photocurrent is polarization independent and can therefore be obtained by unpolarized radiation. In the microscopic theory this photocurrent is mostly due to the Seebeck ratchet effect and is described by the term proportional to χ_1 in Eqs. (21). As an important result, Fig. 5b also reveals that the helicity dependent photocurrent $J_{\mathrm{C}} P_{\mathrm{circ}}(\varphi)$, denoted as circular transverse ratchet effect, contributes a substantial fraction to the total current.

Equations (21) suggest that the ratchet currents display a maximum at normal incidence and are an even function of the angle of incidence. This important macroscopic characteristic of the photocurrent has, in fact, been verified by measuring the polarization dependence of the photocurrent for various angles of incidence θ_0.

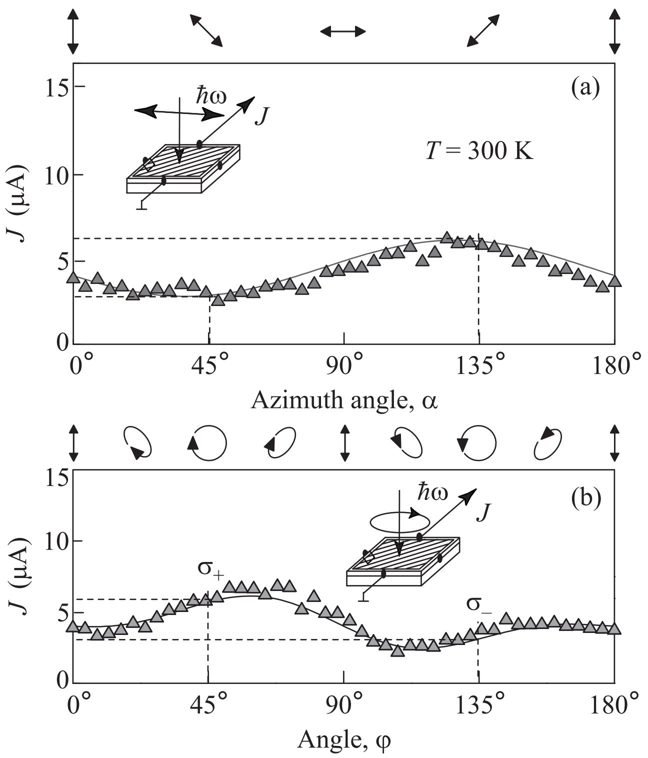

Fig. 5. Photocurrent J generated in sample ST1 by THz radiation at normal incidence. The current is measured at room temperature, excited by radiation with the wavelength $\lambda = 280$ μm and power $P \approx 2$ kW. (a) Photocurrent J measured for linearly polarized radiation as a function of the azimuth angle α. (b) Photocurrent measured as a function of the angle φ defining the radiation helicity. Full lines are fits to Eq. (4) [see also Eq. (21)]. Insets show the experimental geometry. Arrows and ellipses on top of a) and b) indicate the polarization corresponding to various values of α and φ, respectively

Summary. In summary, the deposition of a lateral periodic potential on a low-dimensional semiconductor structure yields a new route to generate THz radiation induced photocurrents. A periodic potential reduces the symmetry of the structure and evokes additional mechanisms of current formation. This directed current constitutes a ratchet effect which is closely related to the one investigated theoretically by Blanter and Büttiker and called the Seebeck ratchet effect. The photocurrent generation is based on the combined action of a spatially periodic in-plane potential and a spatially modulated light. A further access to ratchet effects provides application of polarized radiation resulting in linear or even circular ratchet effect. For the latter one the circularly polarized radiation is crucially needed and the current direction reverses its sign upon switching of radiation helicity from left- to right-handed light and vice versa. Apart from reviewing the experimental state-of-art, we have provided a detailed theoretical description of THz-radiation induced ratchet effects in 2DES with lateral potential in terms of a phenomenological model as well as presented a theoretical approach based on the quasiclassical Boltzmann equation. The proposed theory of the Seebeck ratchet effect is applicable for the non-degenerate Boltzmann statistics and invalid for the low temperature region characterized by the Fermi energy $\varepsilon_{\mathrm{F}} \gg k_{\mathrm{B}} T$. What is even more important, with decreasing temperature in high-mobility structures the electron mean free-path length l_e becomes comparable with and even longer than the lateral superlattice period. This should be accompanied by a changeover from the mechanism related to the in-plane light intensity modulation with $j \propto \bar{I} h_1 V_1$ to the mechanism of photocurrents arising in an asymmetric lateral potential for a homogeneous excitation and obtained by solving the kinetic equation (8) in the fifth-order perturbation theory, namely, the second order in the amplitude of the light electric field E_0 and the third order in the lateral potential, see Ref. [11]. As for the linear and circular photocurrents, one can show that, at low temperature and degenerate statistics, the coefficients γ, χ_2 and χ_3 are given by Eqs. (23) where the ratio $N_0/k_{\rm B}T$ is replaced by $(m^*/\pi\hbar^2)$. This is true provided the Fermi energy E_F exceeds both the photon energy $\hbar\omega$ and the superstructure potential $|V(x)|$ and the inequality $\omega\tau_\varepsilon \gg 1$ is as before satisfied. The measurement of the detailed temperature dependence of the photocurrent, the development of the Seebeck ratchet theory in the case $l_e > d$ and the comparison between theory and experiment is a future task.

Support from DFG (SFB 689), Linkage Grant of IB of BMBF at DLR, RFBR and the Russian Ministry of Education and Sciences is gratefully acknowledged. We are grateful to V.V. Bel'kov for fruitful discussions.

1. F. Jülicher, A. Ajdari, J. Prost, Rev. Mod. Phys. **69**, 1269 (1997).
2. H. Linke (ed.), *Ratchets and Brownian Motors: Basics, Experiments and Applications*, special issue Appl. Phys. A: Mater. Sci. Process. A **75**, 167 (2002).
3. P. Reimann, Phys. Rep. **361**, 57 (2002).
4. P. Hänggi and F. Marchesoni, Rev. Mod. Phys. **81**, 387 (2009).
5. V.I. Belinicher and B.I. Sturman, Usp. Fiz. Nauk. **130**, 415 (1980) [Sov. Phys. Usp. **23**, 199 (1980)].
6. S.D. Ganichev, V.V. Bel'kov, P. Schneider et al., Phys. Rev. B **68**, 035319 (2003).
7. S.D. Ganichev, P. Schneider, V.V. Bel'kov et al., Phys. Rev. B **68**, 081302 (2003).
8. E.L. Ivchenko, *Optical Spectroscopy of Semiconductor Nanostructures* (Alpha Science International, Harrow, UK, 2005).
9. S.D. Ganichev and W. Prettl, *Intense Terahertz Excitation of Semiconductors* (Oxford University Press, Oxford, 2006).
10. A. Lorke et al., Physica B **249**, 312 (1998).
11. L.I. Magarill, Physica E (Amsterdam) **9**, 652 (2001).
12. M.V. Entin and L.I. Magarill, Phys. Rev. B **73**, 205206 (2006).
13. A.D. Chepelianskii, M.V. Entin, L.I. Magarill, and D.L. Chepelyansky, Eur. Phys. J. B **56**, 323 (2007); Physica E (Amsterdam) **40**, 1264 (2008).
14. W. Weber, L.E. Golub, S.N. Danilov et al., Phys. Rev. B **77**, 245304 (2008).
15. A.M. Song et al., Appl. Phys. Lett. **79**, 1357 (2001).
16. A. Sinitsyn, J. Phys.: Condens. Matter 20, 023201 (2008).
17. P. Olbrich, E.L. Ivchenko, R. Ravash et al., Phys. Rev. Lett. **103**, 090603 (2009).
18. M. Büttiker, Z. Phys. B **68**, 161 (1987).
19. Ya.M. Blanter and M. Büttiker, Phys. Rev. Lett. **81**, 4040 (1998).
20. P. Reimann, M. Grifoni, and P. Hänggi, Phys. Rev. Lett. **79**, 10 (1997).
21. I. Zapata, R. Bartussek, F. Sols, and P. Hänggi, Phys. Rev. Lett. **77**, 2292 (1996).
22. F. Berger, T. Schmiedl, and U. Seifert, Phys. Rev. E **79**, 031118 (2009).
23. D. Cubero, V. Lebedev, and F. Renzoni, Phys. Rev. E **82**, 041116 (2010).
24. G.G. Carlo, L. Ermann, F. Borondo et al. (at press).
25. P. Olbrich, E.L. Ivchenko, T. Feil et al., 2008, arXiv:0808.1983v1[cond-mat.mes-hall].
26. P. Olbrich, J. Karch, J. Kamann et al., Phys. Rev. B **83**, 165320 (2011).
27. S.D. Ganichev, S.A. Emel'yanov, and I.D. Yaroshetskii, Pis'ma Zh. Èksp. Teor. Fiz. **35**, 297 (1982) [JETP Lett. **35**, 368 (1982)].
28. S.D. Ganichev, E. Ziemann, Th. Gleim et al., Phys. Rev. Lett. **80**, 2409 (1998).
29. S.D. Ganichev, Ya.V. Terent'ev, and I.D. Yaroshetskii, Pis'ma Zh. Tekh. Fiz **11**, 46 (1985) [Sov. Tech. Phys. Lett. **11**, 20 (1985)].
30. B.E.A. Saleh and M.C. Teich, *Fundamentals of Photonics* (John Wiley & Sons, Inc., 2007).
31. S.D. Ganichev, E.L. Ivchenko, and W. Prettl, Physica E **14**, 166 (2002).
32. D. Weiss, K. v. Klitzing, K. Ploog, and G. Weimann, Europhys. Lett. **8**, 179 (1989).